

Gap solitons of spin-orbit-coupled Bose-Einstein condensates in $\mathcal{PT}$ periodic potential

S Wang(王双), Y H Liu(刘元慧), and T F Xu(徐天赋)

Citation: Chin. Phys. B, 2022, 31 (**7**): 070306. DOI: 10.1088/1674-1056/ac538e
Journal homepage: http://cpb.iphy.ac.cn; http://iopscience.iop.org/cpb

What follows is a list of articles you may be interested in

Anderson localization of a spin-orbit coupled Bose-Einstein condensate in disorder potential

Huan Zhang(张欢), Sheng Liu(刘胜), and Yongsheng Zhang(张永生)
Chin. Phys. B, 2022, 31 (**7**): 070305. DOI: 10.1088/1674-1056/ac538d

Vortex chains induced by anisotropic spin-orbit coupling and magnetic field in spin-2 Bose-Einstein condensates

Hao Zhu(朱浩), Shou-Gen Yin(印寿根), and Wu-Ming Liu(刘伍明)
Chin. Phys. B, 2022, 31 (**6**): 060305. DOI: 10.1088/1674-1056/ac4020

Pseudospin symmetric solutions of the Dirac equation with the modified Rosen—Morse potential using Nikiforov—Uvarov method and supersymmetric quantum mechanics approach

Wen-Li Chen(陈文利) and I B Okon
Chin. Phys. B, 2022, 31 (**5**): 050302. DOI: 10.1088/1674-1056/ac2f33

Manipulating vortices in *F*=2 Bose-Einstein condensates through magnetic field and spin-orbit coupling

Hao Zhu(朱浩), Shou-Gen Yin(印寿根), and Wu-Ming Liu(刘伍明)
Chin. Phys. B, 2022, 31 (**4**): 040306. DOI: 10.1088/1674-1056/ac398f

Topologically protected edge gap solitons of interacting Bosons in one-dimensional superlattices

Xi-Hua Guo(郭西华), Tian-Fu Xu(徐天赋), Cheng-Shi Liu(刘承师)
Chin. Phys. B, 2018, 27 (**6**): 060307. DOI: 10.1088/1674-1056/27/6/060307

Gap solitons of spin–orbit-coupled Bose–Einstein condensates in $\mathcal{PT}$ periodic potential

S Wang(王双)[1], Y H Liu(刘元慧)[2], and T F Xu(徐天赋)[1,†]

[1] *Hebei Key Laboratory of Microstructural Material Physics, School of Science, Yanshan University, Qinhuangdao* 066004, *China*
[2] *School of Science, Yanshan University, Qinhuangdao* 066004, *China*

(Received 17 November 2021; revised manuscript received 25 January 2022; accepted manuscript online 10 February 2022)

We numerically investigate the gap solitons in Bose–Einstein condensates (BECs) with spin–orbit coupling (SOC) in the parity–time ($\mathcal{PT}$)-symmetric periodic potential. We find that the depths and periods of the imaginary lattice have an important influence on the shape and stability of these single-peak gap solitons and double-peak gap solitons in the first band gap. The dynamics of these gap solitons are checked by the split-time-step Crank–Nicolson method. It is proved that the depths of the imaginary part of the $\mathcal{PT}$-symmetric periodic potential gradually increase, and the gap solitons become unstable. But the different periods of imaginary part hardly affect the stability of the gap solitons in the corresponding parameter interval.

Keywords: gap solitons, spin–orbit coupling, $\mathcal{PT}$-symmetric periodic potential

PACS: 03.75.Lm, 67.85.–d, 75.70.Tj **DOI:** 10.1088/1674-1056/ac538e

1. Introduction

Spin–orbit coupling (SOC) is a fundamental effect in quantum mechanics and plays an indispensable role in condensed matter physics.[1–3] However, because of the difficulty of adjusting the coupling in practical materials, there are certain limitations to the adjustable region of SOC strength. As Rashba and Dresselhaus have achieved SOC experimentally,[4] more and more works are enthusiastic about studying SOC effects in BECs system. The new door to the ultra-cold atom quantum system is thus opened, which creates many new possibilities for observing and analyzing quantum phenomena at the macro level. The SOC-BECs effect also shows many interesting localization phenomena, such as solitons,[5–9] band gap solitons[10–12] and vortex structures.[13,14]

The concept of the $\mathcal{PT}$ periodic potential firstly appeared in the study of quantum operators and their spectra.[15,16] In 1998, Bender and Boettcher proposed the idea that some non-Hermitian Hamiltonian can have a real spectrum in the specific parameter domain.[17] Even if the Hamiltonian has a non-Hermitian property, it has a complex potential that follows the $\mathcal{PT}$ periodic potential. The specified potential satisfies $U(x) = U^*(-x)$, thus Hamiltonian can also have a completely real eigen spectrum.[18] The operator $\mathcal{P}$ is the parity reflection operator, representing the space inversion transformation of the quantum state, and $\mathcal{T}$ is the time inversion operator. The effects of the two operators on the coordinate operator x and the momentum operator p are defined as $\mathcal{P}: x \to -x$, $p \to -p$, $\mathcal{T}: \mathrm{i} \to -\mathrm{i}$, $t \to -t$, and $p \to -p$.[19] The $\mathcal{PT}$ periodic potential requires that the complex potential must satisfy the real part as an even function and the imaginary part an odd function. The most interesting feature of this Hamiltonian is the existence of a critical threshold. Beyond this threshold, the $\mathcal{PT}$ symmetry will be broken and the system will undergo a sudden phase transition.[20,21] The pioneering work of Bender and Boettcher has broadened the way for the development of symmetric quantum mechanics. The unique property of $\mathcal{PT}$ symmetry has been introduced into many important fields of physics.[22–27] It has already been realized in optical systems[28,29] and developed into BECs system in recent years.[30–32]

In this article, we carefully analyze the properties of the gap solitons in the SOC-BECs system with the $\mathcal{PT}$ periodic potential. We have discovered a new type of gap solitons in the SOC-BECs system in the $\mathcal{PT}$ periodic potential by the Newton method. The single-peak and double-peak band gap solitons in the first band gap are investigated for their space distribution and stability. We have also researched the influence of the depths and periods of the imaginary part of $\mathcal{PT}$ periodic potential on these gap solitons. We prove that the band gap solitons in the SOC-BECs system with the $\mathcal{PT}$ periodic potential exist steadily in the corresponding band gap. The depth of the imaginary part of the $\mathcal{PT}$ periodic potential affects the stability of the gap solitons in the first band gap, but the period does not produce important influence.

This article is organized as follows. In Section 2, we use the dimensionless coupled Gross–Pitaevskii equation to illustrate the system. In Section 3, we get the linear Bloch spectrum and Bloch waves by solving the equations, and determine the position of the linear band gap. In Section 4, we show the characteristics of the gap solitons with different depths and periods of the imaginary part of the $\mathcal{PT}$-symmetric potential. In Section 5, we discuss the influence of the depths and periods

†Corresponding author. E-mail: tfxu@ysu.edu.cn

© 2022 Chinese Physical Society and IOP Publishing Ltd

of the imaginary part on the stability of the gap solitons. Section 6 is a summary.

2. Theoretical model

Our mean-field model of the SOC-BECs system is given by the one-dimensional coupled Gross–Pitaevskii (GP) equation

$$\begin{aligned} \mathrm{i}\hbar\frac{\partial \Phi}{\partial t} &= \left[-\frac{1}{2m}(\hbar\frac{\partial}{\partial x}-\mathrm{i}m\widetilde{a_l}t)^2-\mathrm{i}\widetilde{\gamma}\frac{\partial}{\partial x}\sigma_z+\widetilde{\delta}\sigma_z+\widetilde{\Omega}\sigma_x\right]\Phi \\ &\quad+\widetilde{V}_{\mathrm{trap}}\Phi+\frac{4\pi\hbar^2\widetilde{a_\mathrm{s}}}{m}(|\Phi_1|^2+|\Phi_2|^2)\Phi, \end{aligned} \tag{1}$$

where $\Phi=(\Phi_1,\Phi_2)^{\mathrm{T}}$ is the total wave function, Φ_1 for up spin component and Φ_2 for down spin component. Here, m is the atom mass and $m\widetilde{a_l}$ represents the force of the vector gauge. The SOC effect occurs in the same direction, and $\{\sigma_i\}$ are the Pauli matrices. The parameter $\widetilde{\gamma}=\hbar k_{\mathrm{Ram}}/m$ represents the SOC coefficient, which is proportional to the wave number of Raman beams k_{Ram}. The parameter $\widetilde{\Omega}$ is the Raman coupling strength, which can be easily adjusted by altering the intensity of the Raman beams. $\widetilde{\delta}$ is the energy detuning. The related s-wave scattering lengths are quantified by $\widetilde{a_\mathrm{s}}$, and because the minor difference between the s-wave scattering lengths can be ignored, we have taken $\widetilde{a_\mathrm{s}}=a_{\mathrm{s}_{11}}=a_{\mathrm{s}_{22}}=a_{\mathrm{s}_{12}}$. $\widetilde{V}_{\mathrm{trap}}$ stands for $\mathcal{PT}$ periodic potential, which takes the form $\widetilde{V}_{\mathrm{trap}}=\widetilde{v_1}\cos^2(k_{\mathrm{lat}}x)+\mathrm{i}\widetilde{v_2}\sin(2qk_{\mathrm{lat}}x)$ throughout this paper. $\widetilde{v_1}$ is the depth of real part potential and $\widetilde{v_2}$ is the depth of imaginary part potential, k_{lat} represents the wave number of lattice beams, and q means the integer wave number multiple of the real and imaginary parts.

To facilitate the calculation, we set Eq. (1) as a dimensionless dynamic equation

$$\begin{aligned} \mathrm{i}\hbar\frac{\partial \Psi}{\partial t} &= \left[-\frac{1}{2}(\frac{\partial}{\partial x}-\mathrm{i}a_l t)^2-\mathrm{i}\gamma\frac{\partial}{\partial x}\sigma_z+\delta\sigma_z+\Omega\sigma_x\right]\Psi \\ &\quad+(v_1\cos^2(x)+\mathrm{i}v_2\sin(2qx))\Psi \\ &\quad+c(|\Phi_1|^2+|\Phi_2|^2)\Psi. \end{aligned} \tag{2}$$

The parameter $c=4\pi n_0\widetilde{a_\mathrm{s}}/k_{\mathrm{lat}}^2$ in Eq. (2) indicates the nonlinear coefficient between two components. These quantities v_1, v_2, Ω and δ are the reduced version of the corresponding parameters. The dimensionless parameters $\gamma=k_{\mathrm{Ram}}/k_{\mathrm{lat}}$ with $\hbar^2k_{\mathrm{lat}}^3/m^2$ as the unit of the reduced accelerated speed a_l. The dimensionless wave-function satisfies $\int \mathrm{d}x(|\Phi_1|^2+|\Phi_2|^2)=1$, and is given by $\Psi=\Phi/\sqrt{n_0}$ with the number density of atoms $n_0=\frac{1}{L}\int \mathrm{d}x(|\Psi_1|^2+|\Psi_2|^2)$. From the above definition, we can get $E_{\mathrm{lat}}=2E_{\mathrm{rec}}$ as the units of time, $E_{\mathrm{rec}}=\hbar^2k_{\mathrm{lat}}^2/(2m)$ as the units of energy and $\hbar/E_{\mathrm{lat}}$ as the units of length, and E_{rec} represents recoil energy of lattice. The amplitude component $\varphi(x)$ is submitted to the time-independent nonlinear Schrödinger equations

$$\begin{aligned} \mu\varphi &= \left[-\frac{1}{2}\frac{\partial^2}{\partial x^2}-\mathrm{i}\gamma\frac{\partial}{\partial x}\sigma_z+\delta\sigma_z+\Omega\sigma_x\right]\varphi \\ &\quad+(v_1\cos^2(x)+\mathrm{i}v_2\sin(2qx))\varphi \\ &\quad+c(|\varphi_1|^2+|\varphi_2|^2)\varphi. \end{aligned} \tag{3}$$

The energy spectrum of the above coupled nonlinear Schrödinger equation consists of this form of Bloch mode $\Psi(x,t)=\varphi(x)\exp(\mathrm{i}a_l tx-\mathrm{i}\mu t)$, where μ represents the chemical potential. The above Eq. (3) can be applied for the case of very small reduced accelerated speed a_l.

3. Linear Bloch spectrum and Bloch waves

Gap solitons exist exclusively in the linear energy gaps, so it is significant to determine these band gaps. In order to achieve the band, we use the Bloch's theorem $\varphi(x)=u_{n,k}(x)\exp(\mathrm{i}kx)$ for the linear version of Eq. (3). Here, u_{nk} means a periodic function, k is the Bloch wave vector and n is the band index. The equation satisfied by u_{nk} is then in the form of

$$\begin{aligned} \mu_{n,k}u_{n,k} &= -\frac{1}{2}\left(\frac{\partial}{\partial x}+\mathrm{i}k\right)^2u_{n,k} \\ &\quad+\left[-\mathrm{i}\gamma\left(\frac{\partial}{\partial x}+\mathrm{i}k\right)\sigma_z+\delta\sigma_z+\Omega\sigma_x\right]u_{n,k} \\ &\quad+(v_1\cos^2(x)+\mathrm{i}v_2\sin(2qx))u_{n,k}. \end{aligned} \tag{4}$$

Solving the above equation by using the plane wave expansion method

$$u_{nk}(x)=\left(\sum_{m=-N}^{N}a_m\mathrm{e}^{\mathrm{i}2mx},\sum_{m=-N}^{N}b_m\mathrm{e}^{\mathrm{i}2mx}\right)^{\mathrm{T}},$$

we can get the linear Bloch spectrum. When the integer wavenumber multiples of the real and imaginary parts are $q=1$, $q=2$ and $q=3$, the band structure of the $\mathcal{PT}$-symmetric potential can all be obtained by solving the following eigenvalue equation:

$$\begin{pmatrix} A_+ & C \\ C & A_- \end{pmatrix}\begin{pmatrix} B \\ D \end{pmatrix}=\mu_{n,k}\begin{pmatrix} B \\ D \end{pmatrix}, \tag{5}$$

where the tridiagonal matrix element $A_\pm(j,j)=\frac{1}{2}(2m+k)^2\pm\delta\pm\gamma(2m+k)+v_1/2$, $A_\pm(j,j+1)=v_1/4+v_2/2$, $A_\pm(j+1,j)=v_1/4-v_2/2$ and the non-diagonal matrix element $C(j,j)=\Omega$.

Figure 1(a) represents the linear Bloch spectrum of the real part of the eigenvalue $\mu_{n,k}$. In the case of the integer wavenumber multiple $q=1$, $q=2$ and $q=3$, it is obvious to see that the curves almost overlap except the individual local part. Figure 1(b) is the spectrum of the imaginary part of the eigenvalue, and shows that the imaginary part of the eigenvalue is 0, which means the energy spectrum is totally real. When the depth of the imaginary part potential v_2 increases to 2, the situation becomes different. As shown in Fig. 2, the real parts of energy spectrum no longer overlap, and the imaginary parts of the eigenvalue have a non-zero value when the integer wavenumber multiples are $q=2$ and $q=3$, so the $\mathcal{PT}$ symmetry is spontaneously broken.

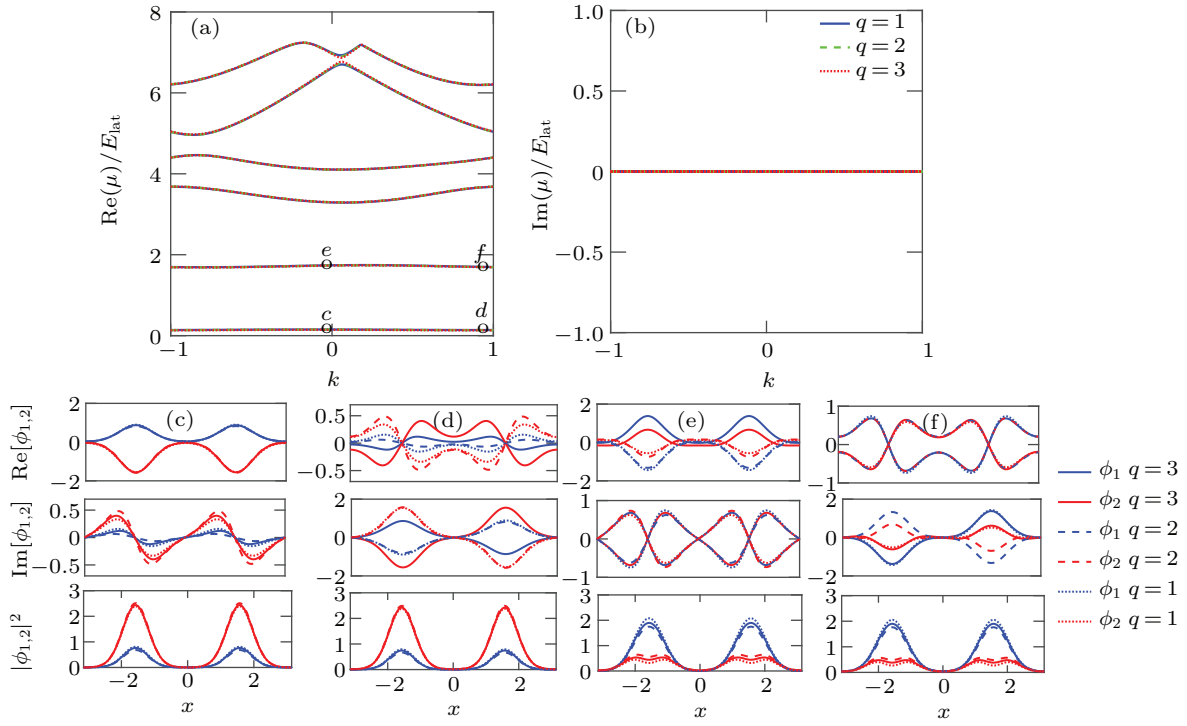


Fig. 1. Linear Bloch spectrum and Bloch waves at the points of the spectrum. (a) and (b) The linear Bloch spectrum for the depth of imaginary part $v_2 = 0.3$. The Bloch waves in the lowest two bands are stated in (c)–(f), the corresponding points shown in (a). Blue lines are for φ_1, while red lines are for φ_2. The other parameters $\Omega = 1$, $\delta = 0.5$, $\gamma = 1$ and $v_1 = 6$ remain the same in this paper.

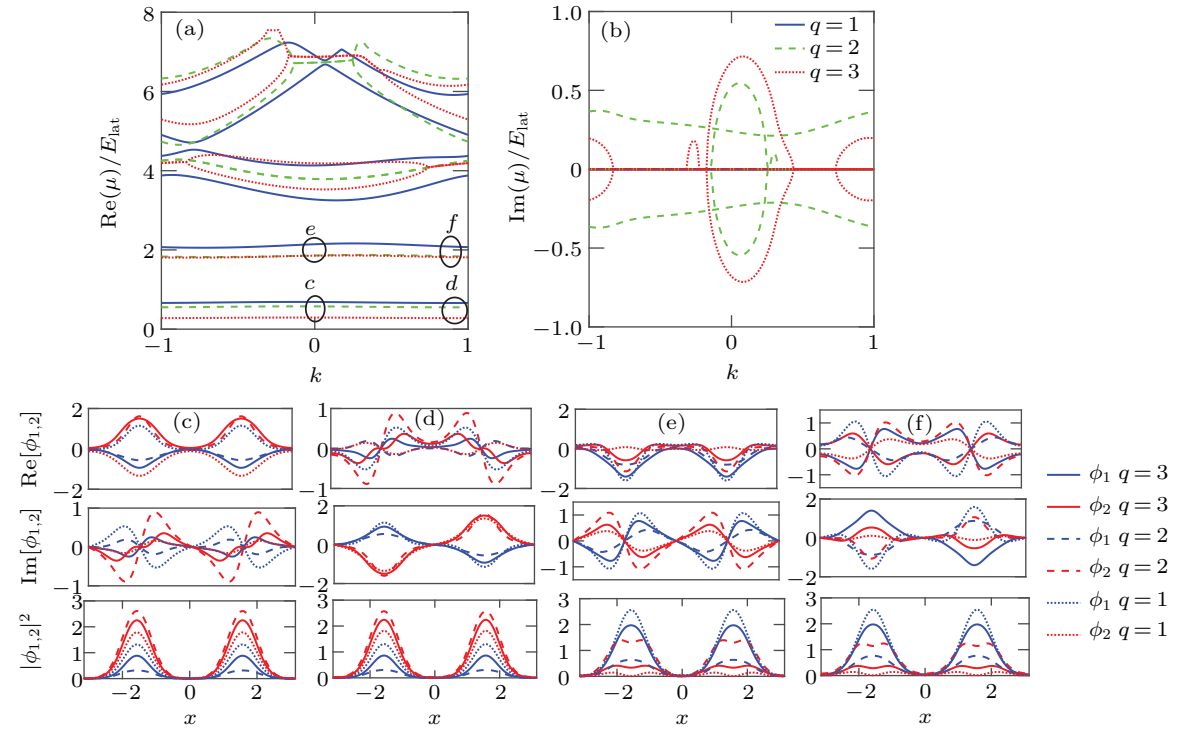


Fig. 2. Linear Bloch spectrum and Bloch waves at the points of the spectrum. (a) and (b) The linear Bloch spectrum for the imaginary potential depth $v_2 = 2$. The Bloch waves in the lowest two bands are indicated in (c)–(f), the corresponding points shown in panel (a). The other parameters are identical to Fig. 1.

In Figs. 1(c)–(f), it can be observed that when the depth of the imaginary part potential is $v_2 = 0.3$, the linear Bloch waves at the spectral symmetry mark points exhibit a weak spin polarization phenomenon. The first component φ_1 dominates in the second band, and the second component φ_2 dominates in the first band. In Figs. 2(c)–2(f), we show the results for the depth of the imaginary part $v_2 = 2$. The spin polarization phenomenon of Bloch waves becomes more obvious for the different value of q, while the spin polarization at $k = 0$ and $k = 1$ of the same energy bands maintains the same. We also analyze the change of v_2 on the spectrum for the different integer wavenumber multiple q, as shown in Fig. 3. It can be observed

from the figure that in the case of the integer wavenumber multiple $q = 1$, with the gradual increase of the depth of imaginary part potential v_2, the bandwidths of the first band gap and the second band gap gradually narrow. When the integer wavenumber multiple is $q = 2$, the first band gap constantly narrows and the second band gap widens step by step. For the case of the integer wavenumber multiple $q = 3$, the first two bands are separated totally with the increase of v_2.

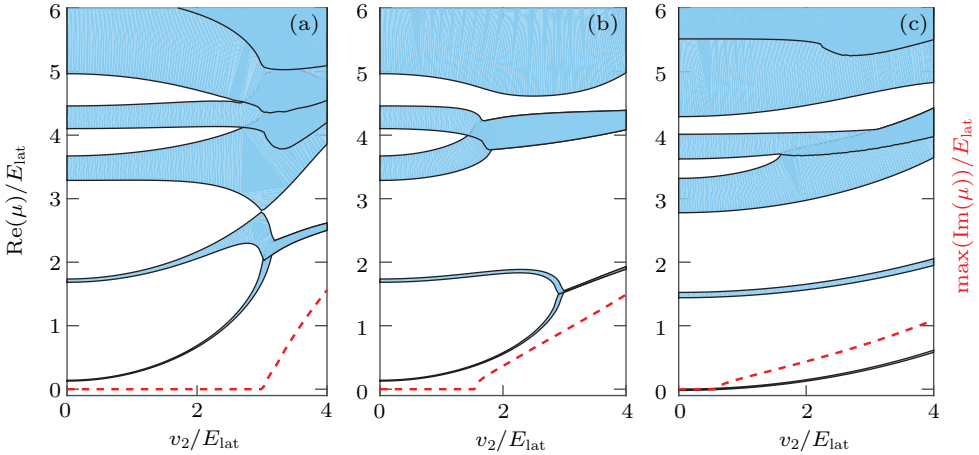


Fig. 3. Linear Bloch spectrum. The filled areas represent the energy bands, the blank areas represent the gaps. (a)–(c) The spectrum of the depth of imaginary part potential v_2 for the integer wavenumber multiple $q = 1$, $q = 2$ and $q = 3$, respectively.

It can be seen from the red dotted line in Fig. 3 that when the integer wavenumber multiple is $q = 1$, the $\mathcal{PT}$ symmetry still exists in the interval $v_2 \leq 3$, so the energy eigenvalue can have a completely real energy spectrum for the case. When the integer wavenumber multiple is $q = 2$, the symmetry is maintained in the interval of $v_2 \leq 1.5$. When the integer wavenumber multiple is $q = 3$, the interval that satisfies the $\mathcal{PT}$ symmetry is getting smaller and smaller. The above analysis results are in full agreement with Fig. 2(b). We can conclude that the broken critical value of $\mathcal{PT}$ symmetry will gradually become smaller with the decrease of the period of the imaginary part potential. In the following content, we will study the existence of the gap solitons in the first band gap for the three cases ($q = 1$, $q = 2$, and $q = 3$) in Fig. 3.

4. Gap solitons

The Newton relaxation method is used to numerically calculate the gap soliton solutions of Eq. (3). First of all, we discretize Eq. (3), set the initial solution, and then fix the chemical potential in the band gap region with the zero boundary condition. The gap solitons of the first and second gaps in the case of the depth of imaginary part $v_2 = 0.3$ and $v_2 = 2$ have been described in Fig. 4. In the first band gap region, there exists one family of fundamental single-peak band gap solitons, named as the first family solitons.[33] In addition, a class of high-order fundamental solitons are also found, which can be understood to advance from the fundamental mode to the composite mode, named as the double-peak gap solitons. With the increase of the depth of the imaginary part v_2, both single-peak gap soliton modes and double-peak soliton modes have bigger norm than when $v_2 = 0.3$, and the norm of the double-peak gap solitons is always stronger than the one of single-peak gap solitons in the (N, μ) plane.

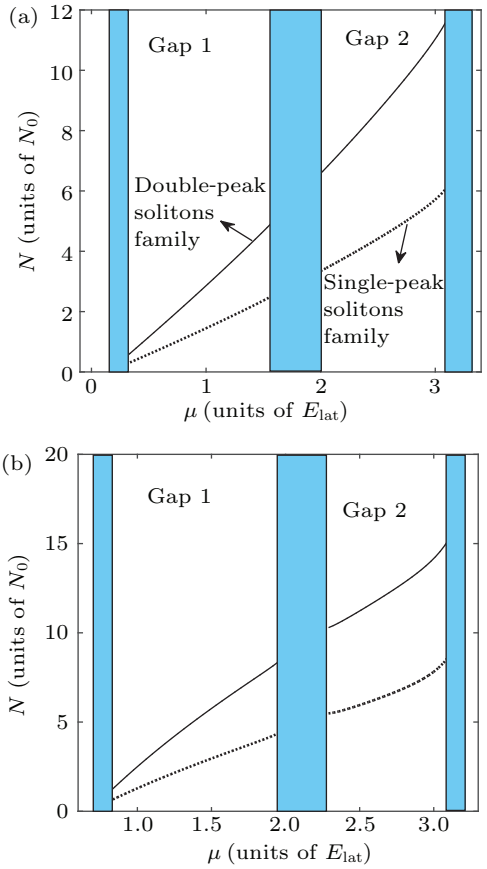


Fig. 4. Gap solitons in the first and second gaps in the (N, μ) plane. The color areas are corresponding to the linear bands. The solid line represents the double-peak gap solitons family, the dotted line represents the single-peak gap solitons family. Panel (a) for the depth of imaginary part $v_2 = 0.3$ and panel (b) for $v_2 = 2$.

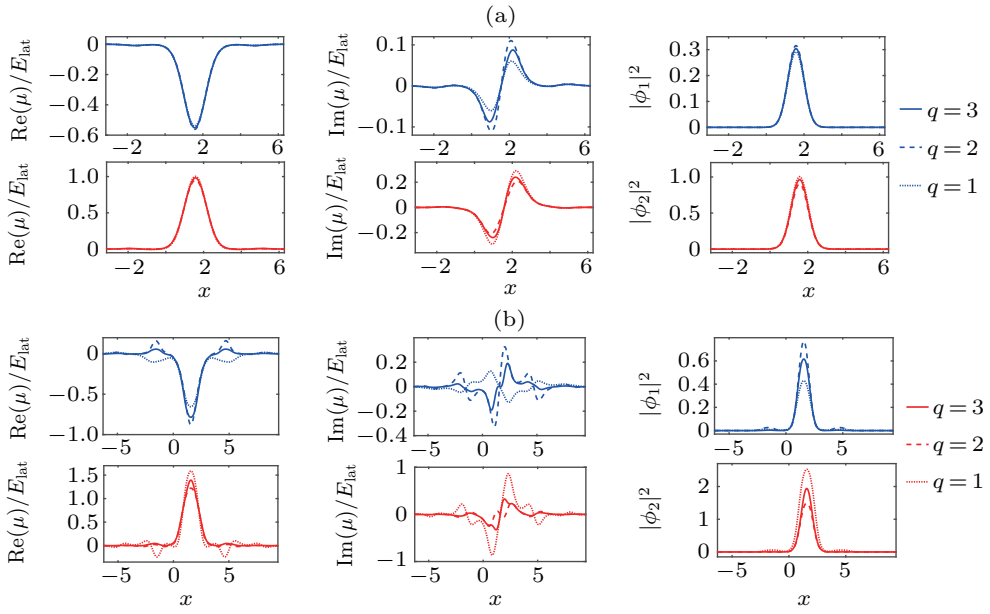


Fig. 5. The density distribution of single-peak gap solitons in the first gap for the case of the integer wavenumber multiple $q=1$, $q=2$ and $q=3$. Here, the depth of imaginary part $v_2=0.3$ is used in panel (a). In panel (b) the depth of the imaginary part is $v_2=2$.

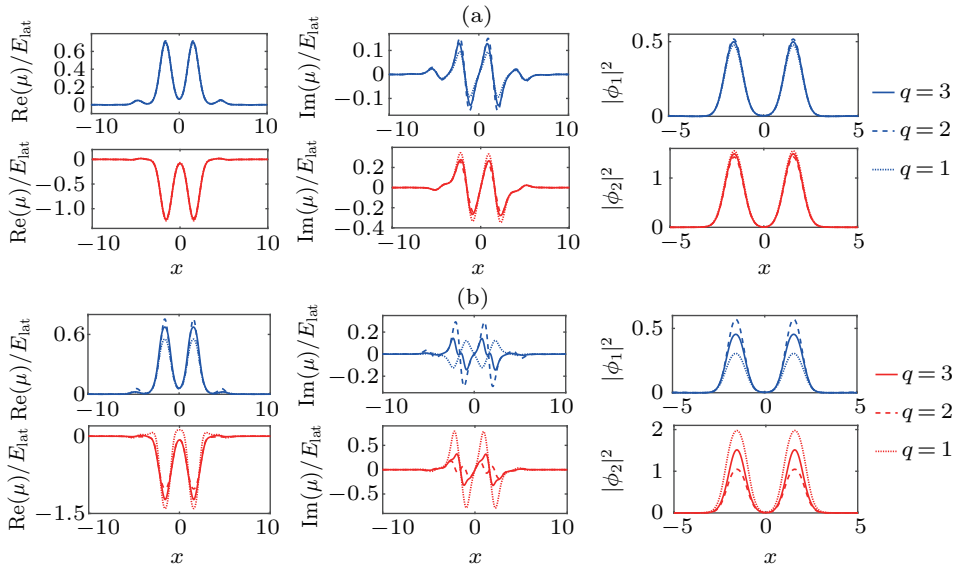


Fig. 6. The density distribution of double-peak gap solitons in the first gap for the case of the integer wavenumber multiple $q=1$, $q=2$ and $q=3$. Here, the depth of imaginary part $v_2=0.3$ is used in panel (a). In panel (b) the depth of the imaginary part is $v_2=2$.

The density distribution of the single-peak gap solitons is shown in Fig. 5. It is very obvious that the single-peak gap solitons have parity symmetry in Fig. 5(a). As the depth of the imaginary part v_2 increases to 2, the gap solitons transform into spin polarization, as shown in Fig. 5(b). Figure 6 shows the density distribution of double-peak gap solitons. We can see that this dipole mode is a composite structure comprising two modes of the same phase. When the depth of the imaginary part is $v_2=2$, the double-peak gap solitons have also been polarized. It can be observed from Figs. 5 and 6 that the amplitude of the gap solitons grows with the increase of the depth of the imaginary part v_2, but the parity symmetry does not change.

5. Analysis of solitons stability

The stability analysis is crucial for the gap soliton solutions. Because it is about whether it is observable in the experiment. In this chapter, the influence of the depth and period of the imaginary part of the $\mathcal{PT}$-symmetric potential on the stability of the gap solitons is mainly analyzed by using the split-step Crank–Nicolson method.[34] In order to excite the perturbation, a Gaussian random noise is superimposed on the gap solitons, then the overall waveform is used as the initial value and begins to evolve in Eq. (3). We first set the integer wavenumber multiple $q=1$ for the single-peak gap solitons family of the first band gap, and the stability analysis results are shown in Figs. 7(a) and 7(b). It can be clearly seen that when the depth of the imaginary part is $v_2=0.3$, the first fam-

ily gap solitons are linearly stable in Fig. 7(a). As the depth of imaginary part v_2 increases to 2, the gap solitons are linearly unstable in Fig. 7(b). The result is as the same for the double-peak gap solitons as shown in Figs. 7(c) and 7(d). Dynamic evolution is stable for the depth of the imaginary part $v_2 = 0.3$ and unstable for $v_2 = 2$. Through precise analysis, it is found that this situation also applies to the integer wavenumber multiples $q = 2$ and $q = 3$.

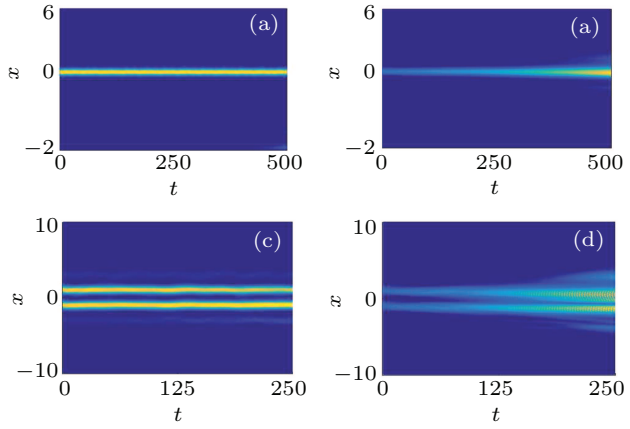


Fig. 7. Time evolution of gap solitons in the first gap. The initial wave functions are the gap solitons solutions with Gaussian distributed noise added on. (a) A stable evolution of single-peak gap solitons in the first band gap at $v_2 = 0.3$. (b) An unstable evolution of single-peak gap solitons in the first band gap at $v_2 = 2$. (c) A stable evolution of double-peak gap solitons in the first band gap at $v_2 = 0.3$. (d) An unstable evolution of double-peak gap solitons in the first band gap at $v_2 = 2$. For all panels, the chemical potential is $\mu = 1$.

6. Conclusion

We have researched the properties of gap solitons in SOC-BECs system with $\mathcal{PT}$-symmetric potential. The linear energy spectrum and Bloch waves for the different depths and periods of the imaginary part of $\mathcal{PT}$-symmetric potential are carefully investigated. Two types of gap solitons are obtained numerically in the first band gap, namely, the single-peak gap solitons and double-peak gap solitons. The increase of the depth of the imaginary potential causes the two kinds of gap solitons to become spin-polarized notably and grow in amplitude. Finally, the method of the real-time evolution with the noise is used to analyze the dynamic evolution of the corresponding gap solitons. It is found that when the depth of imaginary part of $\mathcal{PT}$-symmetric potential increases, the gap solitons gradually become unstable. While the variation of the period of the imaginary part does not change the stability of the gap solitons for the parameter interval.

Acknowledgement

This work is supported by Science and Technology Project of Hebei Education Department, China (Grant No. ZD2020200).

References

[1] Achilleos V, Frantzeskakis D J, Kevrekidis P G and Pelinovsky D E 2013 *Phys. Rev. Lett.* **110** 264101
[2] Kato Y K, Myers R C, Gossard A C and Awschalom D D 2004 *Science* **306** 1910
[3] Xiao D, Chang M C and Niu Q 2010 *Rev. Mod. Phys.* **82** 1959
[4] Dresselhaus G 1955 *Phys. Rev.* **100** 580
[5] Pedri P and Santos L 2005 *Phys. Rev. Lett.* **95** 200404
[6] Kartashov Y V, Konotop V V and Zezyulin D A 2014 *Phys. Rev. A* **90** 063621
[7] Xu T F, Zhang Y F, Xu L C and Li Z D 2017 *Chin. Phys. B* **26** 100304
[8] Xu T F, Li W L, Li Z D and Zhang C 2018 *Chaos Soliton Fract.* **111** 62
[9] Xu T F 2018 *Chin. Phys. B* **27** 016702
[10] Ostrovskaya E A and Kivshar Y S 2003 *Phys. Rev. Lett.* **90** 160407
[11] Desyatnikov A S, Ostrovskaya E A, Kivshar Y S and Denz C 2003 *Phys. Rev. Lett.* **91** 153902
[12] Louis P J, Ostrovskaya E A, Savage C M and Kivshar Y S 2003 *Phys. Rev. A* **67** 013602
[13] Liu C F, Yu Y M, Gou S C and Liu W M 2013 *Phys. Rev. A* **87** 063630
[14] Fetter A L 2014 *Phys. Rev. A* **89** 023629
[15] Bender C M, Brody D C and Jones H F 2002 *Phys. Rev. Lett.* **89** 270401
[16] Longhi S 2009 *Phys. Rev. Lett.* **103** 123601
[17] Bender C M, Brody D C and Jones H F 2004 *Phys. Rev. Lett.* **93** 251601
[18] Bender C M and Boettcher S 1998 *Phys. Rev. Lett.* **80** 5243
[19] Makris K G, El-Ganainy R, Christodoulides D N and Musslimani Z H 2008 *Phys. Rev. Lett.* **100** 103904
[20] Nixon S and Yang J 2015 *Phys. Rev. A* **91** 033807
[21] Ramezani H, Kottos T, El-Ganainy R and Christodoulides D N 2010 *Phys. Rev. A* **82** 043803
[22] Musslimani Z H, Makris K G, El-Ganainy R and Christodoulides D N 2008 *Phys. Rev. Lett.* **100** 030402
[23] Guo A, Salamo G J, Duchesne D, Morandotti R, Volatier-Ravat M, Aimez V and Christodoulides D N 2009 *Phys. Rev. Lett.* **103** 093902
[24] Makris K G, El-Ganainy R, Christodoulides D N and Musslimani Z H 2010 *Phys. Rev. A* **81** 063807
[25] Konotop V V, Yang J and Zezyulin D A 2016 *Rev. Mod. Phys.* **88** 035002
[26] Jia C Y and Liang Z X 2020 *Chin. Phys. Lett.* **37** 040502
[27] Cao Y and Cao J 2021 *Chin. Phys. Lett.* **38** 080202
[28] Jones H F 2012 *J. Phys. A: Math. Theor.* **45** 135306
[29] Christodoulides D N, Lederer F and Silberberg Y 2003 *Nature* **424** 817
[30] Graefe E M, Korsch H J and Niederle A E 2008 *Phys. Rev. Lett.* **101** 150408
[31] Graefe E M, Korsch H J and Niederle A E 2010 *Phys. Rev. A* **82** 013629
[32] Single F, Cartarius H, Wunner G and Main J 2014 *Phys. Rev. A* **90** 042123
[33] Zhang Y, Liang Z and Wu B 2009 *Phys. Rev. A* **80** 063815
[34] Zhou H, Douvenot R and Chabory A 2020 *J. Comput. Phys.* **402** 109042